RESEARCH ARTICLE

Key Points:
- EPB development significantly enhanced along the meridian 120°E/60°W during the September 2017 geomagnetic storm
- The enhanced EPBs along the meridian are mainly due to the PPEFs resulting from two large southward excursions of IMF *Bz*
- The westward drifts increasing with latitude/altitude produced west-tilted structures of EPBs in the Asian sector

Correspondence to:
G. Li,
gzlee@mail.iggcas.ac.cn

Storm-Enhanced Development of Postsunset Equatorial Plasma Bubbles Around the Meridian 120°E/60°W on 7–8 September 2017

Guozhu Li[1,2] , Baiqi Ning[1,3], Chi Wang[4], M. A. Abdu[5] , Yuichi Otsuka[6], M. Yamamoto[7] , Jian Wu[8], and Jinsong Chen[8]

[1]Key Laboratory of Earth and Planetary Physics, Institute of Geology and Geophysics, Chinese Academy of Sciences, Beijing, China, [2]College of Earth and Planetary Sciences, University of Chinese Academy of Sciences, Beijing, China, [3]Beijing National Observatory of Space Environment, Institute of Geology and Geophysics, Chinese Academy of Sciences, Beijing, China, [4]State Key Laboratory of Space Weather, National Space Science Center, Chinese Academy of Sciences, Beijing, China, [5]Instituto Nacional de Pesquisas Espaciais (INPE), Sao Jose dos Campos, Brazil, [6]Institute for Space-Earth Environmental Research, Nagoya University, Nagoya, Japan, [7]Research Institute for Sustainable Humanosphere, Kyoto University, Uji, Japan, [8]National Key Laboratory of Electromagnetic Environment, Research Institute of Radio Wave Propagation, Qingdao, China

Abstract Storm time development of equatorial plasma bubbles (EPBs) around the meridian 120°E/60°W during early September 2017, when the *Bz* component of interplanetary magnetic field (IMF) experienced two large southward excursions, producing a strong geomagnetic storm that included two main phase decreases, was investigated. The observations from networks of Global Navigation Satellite Systems total electron content receivers, very high frequency radars, and ionosondes operated around the meridian reveal that in the American and Asian sectors, intense EPB irregularities developed and extended to dip latitudes of ~30°N and 46°N, respectively, following rapid sunset *F* layer height rises during two episodes of strong southward IMF *Bz* excursions. The storm-enhanced EPB irregularities, however, were not observed following the sunset terminator in the Pacific sector, where the sunset rise of *F* layer was not detected. More interestingly, the EPBs in the Asian sector were observed to drift toward the west, with velocity increasing from ~30 m/s at low latitude to ~95 m/s at middle latitude. The poleward increasing westward drifts drove the formation of west-titled structure of irregularities. For the EPBs in the American sector, no apparent west-tilted structure was detected. The results indicate that the prompt penetration undershielding electric fields (PPEF) of eastward polarity resulting from the two IMF *Bz* southward excursions dominated the generation of postsunset EPBs in the American and Asian sectors, respectively. The westward drifts of PPEF-induced EPBs in the Asian sector could be attributed dominantly to disturbance westward wind, with a possible contribution to it arising from the PPEF.

Plain Language Summary The development and evolution of equatorial plasma bubbles (EPBs) exhibit complex global behavior during geomagnetic storms. In recent years, an international space weather meridian circle program, which aims to provide a global picture of unfolding space weather events by using diverse instruments along the approximate meridian 120°E/60°W, that is, the Asian and American longitude sectors, was launched. Considering the sunset interval (~12 hr) between the two longitudes, it is expected that the development of postsunset EPBs, if enhanced in one region by short-lived prompt penetration electric fields (PPEF), would be inhibited in the other region under the delayed and long duration effect of disturbance dynamo electric fields. Here we report a unique case of significantly enhanced postsunset EPBs developments by PPEF in both the American and Asian sectors, but their total absence by disturbance dynamo electric fields in the Pacific sector during the September 2017 geomagnetic storm sequence. Moreover, the PPEF-induced EPBs along the meridian show different characteristics, with apparent west-tilted structure in the Asian sector but not in the American sector. This sort of study based on the international space weather meridian circle program observations will strengthen our understanding on the generation and evolution characteristics of EPBs during geomagnetic storms.

1. Introduction

Equatorial plasma bubbles (EPBs) are plasma depleted flux tubes in the equatorial ionosphere that contain irregularity structures in spatial scales ranging from centimeters to hundreds of kilometers, and also known

as equatorial spread F (ESF), that often produce severe ionospheric scintillations. With their development initiated at the bottom-side density gradient region of a rapidly rising F layer after sunset, the EPBs rise to higher altitudes, above the F layer peak to extend to a wide-latitude band along the magnetic field lines (e.g., Kelley, 2009). Although the EPBs have been studied for several decades, they continue to be an important topic in space weather research, due to their significant impacts on space-based operational systems, such as causing loss-of-lock on satellite to ground links and the difficulty to predict when and where the EPBs will occur under different conditions (e.g., Abdu, 2012).

In recent years, a number of studies on the longitudinal and latitudinal variations of EPBs during geomagnetic storms have been performed. It was revealed that the EPB development can be totally suppressed, be confined to a limited longitude/latitude range, be significantly enhanced to extend to middle latitudes, or be triggered successively in a large longitude region (e.g., Abdu et al., 2003; Carter et al., 2016; Li et al., 2009, 2010; Patra et al., 2016; Tulasi Ram et al., 2008). In East Asia, observations have shown that storm time midlatitude plasma bubble is not a rare phenomenon (e.g., Li et al., 2009; Ma & Maruyama, 2006; Sahai et al., 2009), whereas in the European sector, the first detection of midlatitude plasma bubble was reported more recently (Cherniak & Zakharenkova, 2016; Katamzi-Joseph et al., 2017). Regarding the longitudinal variation of storm time EPBs, there are a few studies that reported substantial differences in EPB activity at nearby longitudes (e.g., Basu et al., 2001; Li et al., 2009). While storm time EPBs were observed mostly to be confined at narrow longitudes, Li et al. (2010), by using observations from a set of in situ satellite and ground-based instruments during the storm period July 2004, reported an unusual case where EPBs occurred following the sunset terminator at a large stretch of longitude region extending more than 180°, from American to Asian sectors. Such longitudinal extension of EPBs under storm time conditions was believed to be associated with long duration of electric field penetration to the equatorial ionosphere.

Instead of the normal eastward drifts of postsunset EPBs on geomagnetic quiet days, storm time observations showed that the eastward drifts of postsunset EPBs can reverse to westward (e.g., Abdu et al., 2003; Ghodpage et al., 2018). During the super storm period 8–10 November 2004, significant westward drifts of EPBs, with maximum velocities of about 80 and 200 m/s, were detected at Chinese and Peruvian longitude sectors, respectively (e.g., Basu et al., 2010; Li et al., 2009). These westward drifts, which occurred during the recovery phase of the storm, were suggested to be induced by the thermospheric disturbance westward winds. During the storm of 26 August 1998, Abdu et al. (2003) found that the initially weak eastward drifts of the postsunset EPBs in the American longitude sector steadily reversed to westward. The zonal plasma drift reversal, however, was suggested to be driven in part also by a vertical Hall electric field induced by the primary zonal penetration electric field. More cases of storm time zonal drifts reversal (from eastward to westward) due to the Hall electric field over Brazil were studied by Santos et al. (2016).

The development and evolution of EPBs exhibit complex global behavior during geomagnetic storms. In recent years, an international space weather meridian circle program, which aims to provide a global picture of unfolding space weather events by using diverse instruments along the approximate meridian circle 120°E/60°W, that is, the Asian and American longitude sectors, was launched. On 7–8 September 2017, a large geomagnetic storm occurred due to a sequence of coronal mass ejections. This storm was characterized by two main phase Dst decreases driven correspondingly by two episodes of rapid and large southward excursions in the Bz component of interplanetary magnetic field (IMF), around 2040–2340 UT on 7 September and 1135–1155 UT on 8 September, respectively. The response of ionospheric total electron content (TEC) and the latitudinal extent of EPBs over China during the storm period have been investigated (Aa et al., 2018; Jin et al., 2018; Lei et al., 2018). The objective of this study is to comparatively investigate the development and evolution of postsunset EPBs in the Asian and American longitudes during the storm. Considering the sunset interval (~12 hr) between the two longitudes, it is expected that the development of postsunset EPBs, if enhanced in one region by short-lived prompt penetration electric field (PPEF) during the development phase in a storm sequence, would be inhibited in the other region under the delayed and long duration effect of a disturbance dynamo electric field (DDEF). In this study we report a unique case of significantly enhanced postsunset EPB developments in both the American and Asian sectors, but their total absence in the Pacific sector during the September 2017 geomagnetic storm sequence. The EPBs observed in the two longitudes show different evolution characteristics. Possible factors responsible for the enhanced development of EPBs and their evolutions along the approximate meridian 120°E/60°W, and the absence of EPB in the Pacific sector, are discussed.
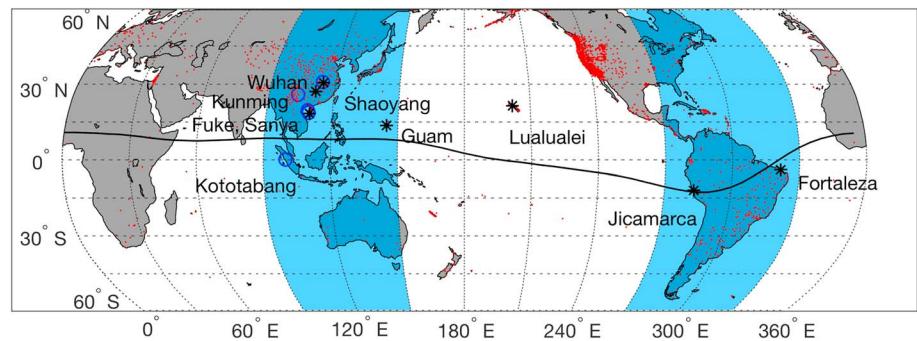
Figure 1. The geographic distribution of the Global Navigation Satellite Systems total electron content receivers (red dots), ionosondes (black asterisks), and very high frequency radars (blue circles).

2. Instruments and Data Processing

In this study, we use ground-based Global Navigation Satellite System (GNSS) ionospheric TEC receivers, very high frequency (VHF) radars, and ionosondes to investigate the occurrence characteristics of EPBs during the September 2017 geomagnetic storm. Some of the instruments are from the Chinese meridian project (Wang, 2010). Figure 1 shows the geographic distributions of the three types of instruments, represented with red dots, blue circles, and black asterisks, respectively. The EPBs detected by these instruments are, in general, shown as fast and significant TEC bite-outs, backscatter plumes, and ionosonde diffuse echoes, respectively (Kelley, 2009).

Total electron content data from two GNSS receiver networks, including the International GNSS Service and the China Crust Movement Observation Network, are used to measure the rate of TEC change index (ROTI). The ROTI, first proposed by Pi et al. (1997), has been employed to detect the occurrence of EPB irregularities, with a threshold value of 0.075 TECu/min (Nishioka et al., 2008). Using a procedure similar to that described in Li et al. (2010), the maps of EPB occurrence rates are constructed based the number of samples with ROTI $\geq$0.075 TECu/min that is divided by the total number of ROTI samples at premidnight (1800–2400 LT) for each grid point (separated 3° in geographic longitude and latitude).

Very high frequency radar multibeam steering observations over Sanya (18.3°N, 109.6°E; dip lat. 13.5°N), Fuke (19.3°N, 109.1°E; dip lat. 14.7°N), and Kototabang (0.2°S, 100.3°E; dip lat. 9.2°S) and fixed beam (due north) observations over Kunming (25.5°N, 103.8°E; dip lat. 22.4°N) and Wuhan (30.5°N, 114.3°E; dip lat. 28.2°N) are used to investigate the onset and evolution characteristics of EPBs in East/Southeast Asia. The five VHF radars, with operational frequencies of 47.5, 47, 47, 45.9, and 48.2 MHz, and peak powers of 24, 54, 100, 24, and 24 kW, respectively, have the ability to detect ionospheric 3-m irregularities associated with EPBs. In this study, the Fuke, Kototabang, and Sanya radars are steered in 7, 16, and 5 directions, with temporal (range) resolutions of about 2, 1.5, and 5 min (0.7, 2.4, and 2.55 km), respectively. Detailed information about the five radars and their operational parameters are given in previous works (e.g., Fukao et al., 2003; Jin et al., 2018; Li et al., 2016, 2017; Zhou et al., 2018) and will not be shown here.

Ionosonde data used in this study are obtained from the stations Fortaleza (3.9°S, 321.6°E; dip lat. 9.7°S), Jicamarca (12°S, 283.2°E; dip lat. 0.2°S), Lualualei (21.4°N, 201.9°E; dip lat. 21.5°N), Guam (13.6°N, 144.9°E; dip lat. 6.3°N), Shaoyang (27.1°N, 111.3°E; dip lat. 24.2°N), and Sanya, which are situated in the American, Pacific, and Asian sectors, respectively. The occurrence of EPBs in ionograms was manually identified as range spreading *F* layer traces. The peak heights of *F* layer (hmF2) were manually scaled by using the SAO explorer software.

3. Results

We first present the IMF *Bz*, AE, SYM/H, and *Kp* indices on 6–8 September in Figure 2. The IMF *Bz* presented two rapid and large southward excursions, reaching about −31 and −17 nT at 2335 UT and 1155 UT on 7 and 8 September, respectively. For the first southward excursion, the SYM/H experienced a rapid reduction from −21 to −90 nT, at a mean rate of −5 nT/min (during 2318–2332 UT), and reached a minimum of
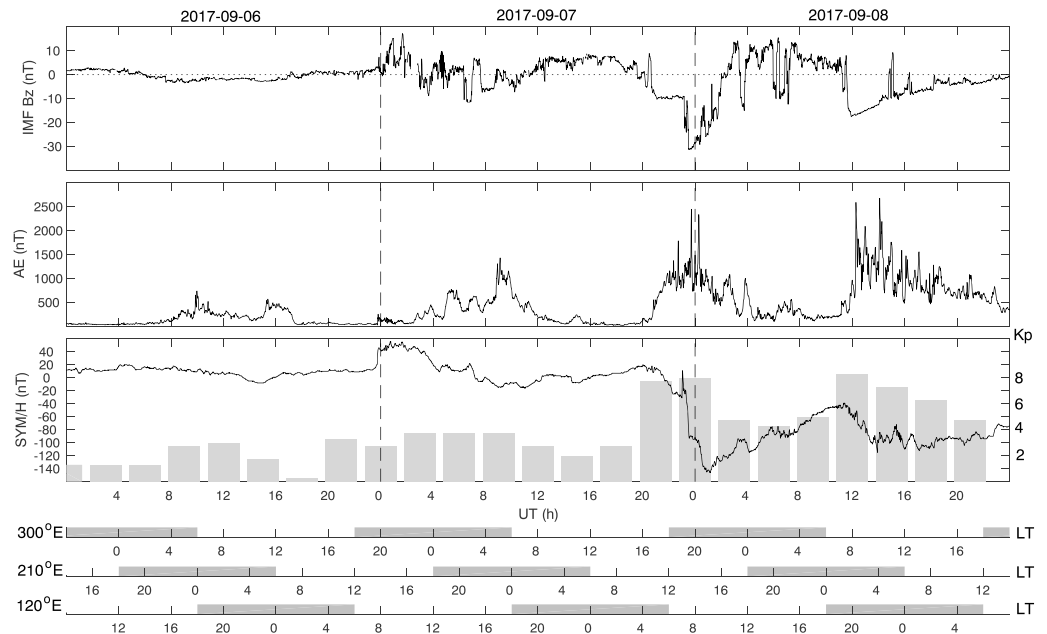
Figure 2. The interplanetary magnetic field *Bz*, AE, SYM/H, and *Kp* indexes during 6–8 September 2017. The axes in the bottom show the corresponding local time in the American (300°E), Pacific (210°E), and East Asian (120°E) sectors, respectively.

−146 nT at 0108 UT on 8 September. The *Kp* attained a value of 8. While the storm was recovering, the SYM/H got intensified again corresponding to the second large southward excursion of IMF *Bz* that occurred at 1136 UT on 8 September, with the SYM/H attaining −115 nT at 1356 UT and the *Kp* reaching 8+. Based on observations from the GNSS TEC receiver—the VHF radar—and the ionosonde networks (Figure 1) during the storm period, we have studied the occurrence characteristics of EPBs around the world, with special focus on the onset conditions and evolution of EPBs in the American and Asian sectors.

Figure 3 shows an overview of irregularity occurrence rates during the period 6–9 September 2017. The irregularity occurrence rates were calculated using ROTI values during premidnight hours (1800–2400 LT) at each grid point. The UT interval of the data points decreases with increase in longitude. The blank areas in the maps represent the regions where the irregularity occurrence rates are not calculated, because there are only few ROTI samples (less than 20) available for each grid. The red thin dots and green circles mark the locations of GNSS TEC receivers and ionosondes, respectively. The solid line represents the magnetic equator. On the geomagnetic quiet day 6 September, the irregularities were not observed in the Asian sector and were confined at low latitudes around the magnetic equator in the Pacific and American longitudes, respectively. A prominent feature seen from Figure 3 is that in the American and Asian sectors, the irregularity occurrence rates on 8 September (corresponding to the two main phase SYM-H decreases of the storm) were significantly higher than those on other days. The irregularities covered a large area in latitude, extending to low and middle latitudes of ~25°N (dip lat. 30°N) and 45°N (dip lat. 46°N) in the American and Asian sectors, respectively. However, in the Pacific sector, no irregularities were observed after sunset on 8 September.

The presence and absence of irregularities seen from the occurrence maps on 8 September are verified by ionosonde observations in the American (Jicamarca and Fortaleza), Pacific (Guam and Lualualei), and Asian (Sanya and Shaoyang) sectors. Six samples of ionograms from the ionosondes are plotted in Figure 4. At Fortaleza and Jicamarca, strong range-type spread *F* (a signature of EPB irregularities in ionograms) were observed around 2310 UT and 2335 UT on 7 September, with durations of about 8 and 11 hr, lasting until 0700 UT and 1100 UT on 8 September, respectively. In the Asian sector, ionograms from the Sanya and Shaoyang ionosondes recorded EPB irregularities during 1230–2030 UT and 1252–1642 UT on 8 September, respectively. In the Pacific sector, the ionograms at Guam and Lualualei did not record the presence of postsunset EPBs on 8 September.
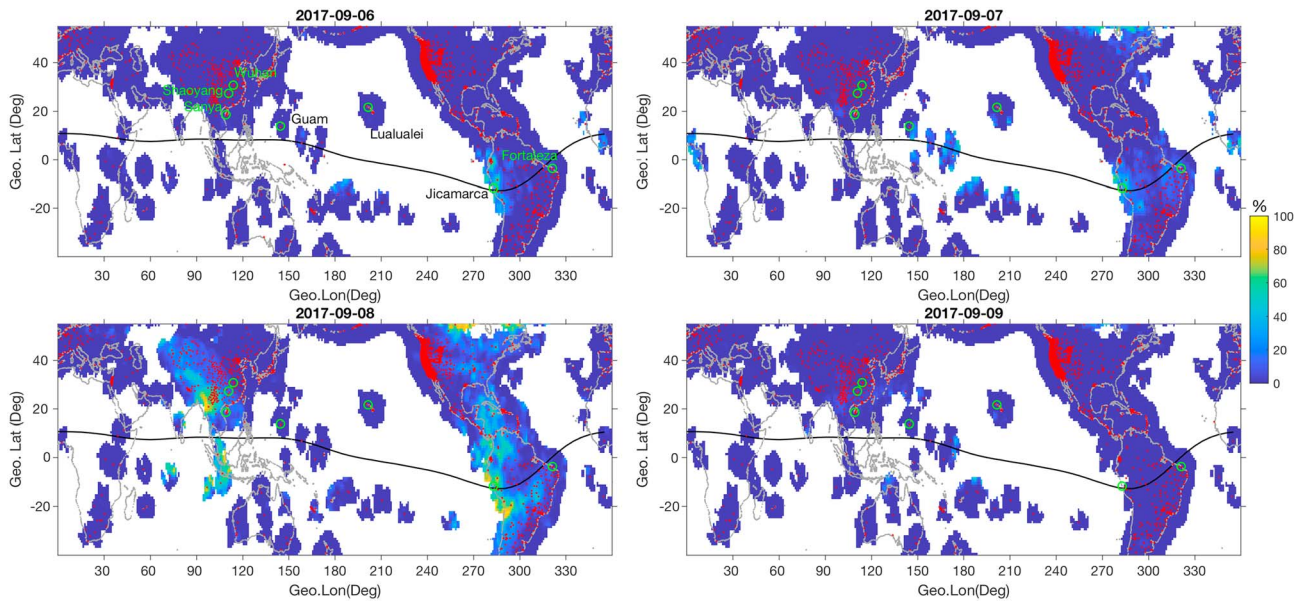
Figure 3. Maps of irregularity occurrence rates during 6–9 September 2017, calculated as the rate of total electron content (TEC) change index values during premidnight hours (1800–2400 LT) at each grid point in the map. The superimposed red dots and green circles mark the locations of TEC receivers and ionosondes, respectively.

To reveal the onset and evolution characteristics of EPBs in the American and Asian sectors, a sequence of ROTI maps at 15-min intervals on 8 September are plotted in Figures 5 and 6, respectively (in Figure 5 the plot starts at 2230 UT on 7 September). The red, yellow, and purple dots represent the ROTI above thresholds of 0.075, 0.3, and 0.5 TECu/min, respectively. Figure 5 shows that in the American sector, two types of
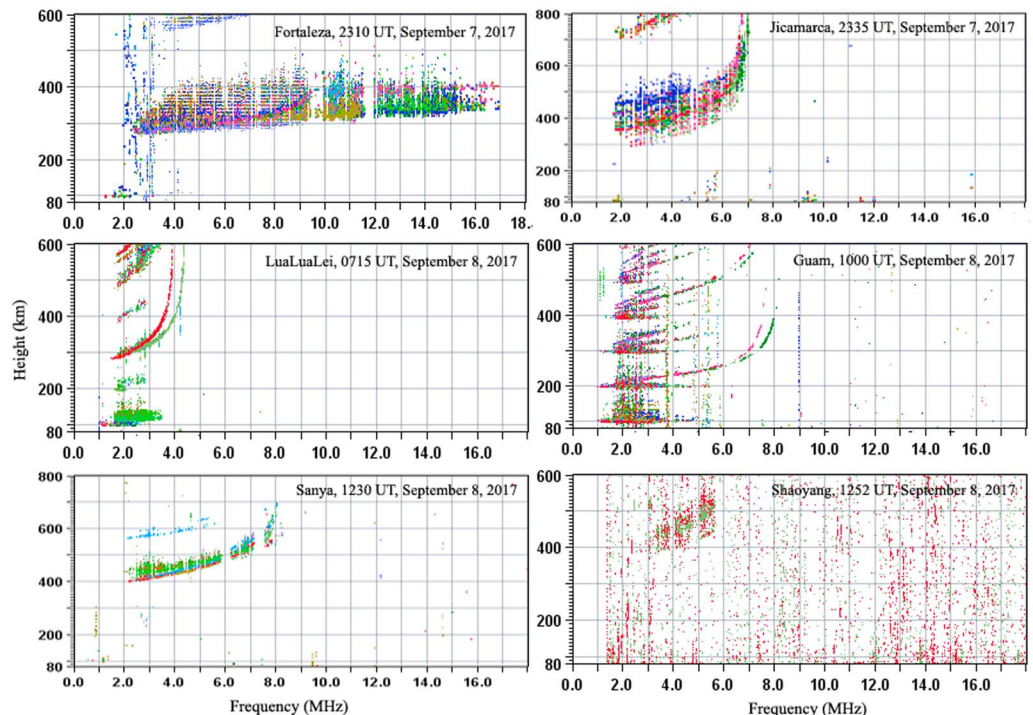

Figure 4. Selected ionograms showing the presence/absence of equatorial plasmabubbles over Fortaleza, Jicamarca, Lualualei, Guam, Sanya, and Shaoyang.
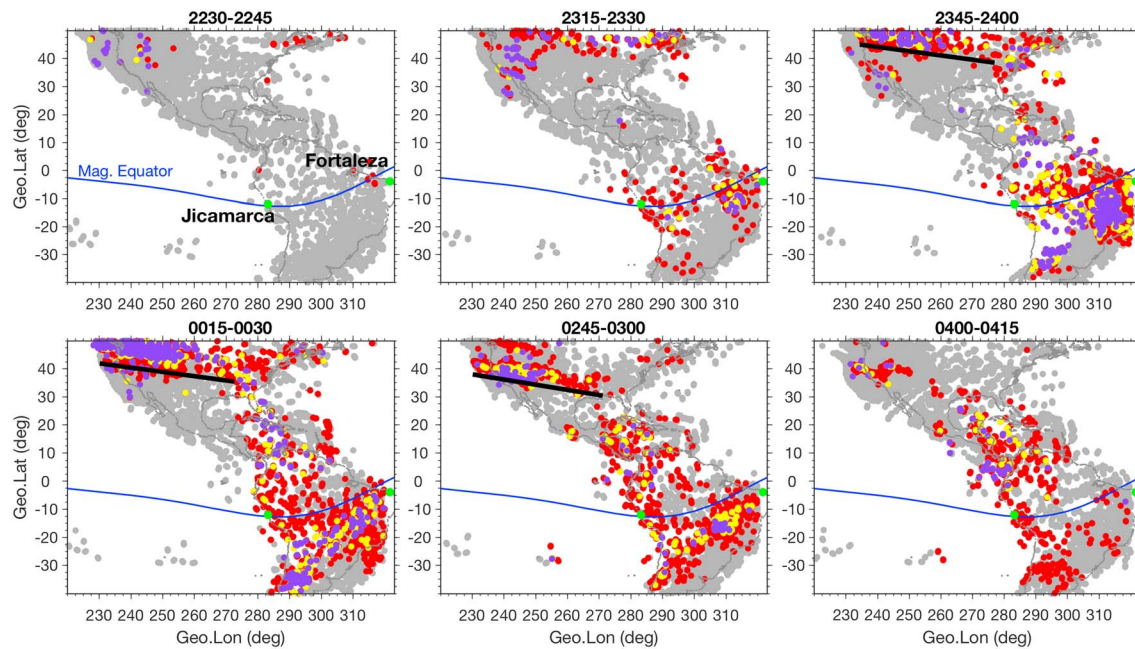
Figure 5. Rate of total electron content change index maps at selected time intervals (on 7–8 September) in the American sector. The green dots mark the locations of the two ionosondes. The superimposed black slant line marks the irregularity structure aligned along the northwest-southeast direction.

irregularities were observed at higher and lower latitudes. The significantly enhanced intensity represented by the purple dots first appeared at higher latitude (above 40°N, dip lat. 47°N) starting around 2245 UT and extended in latitude in the subsequent maps till 0030 UT. These structures appear to be in immediate response to the first Bz southward excursion near 2040 UT on 7 September (Figure 2). They are not associated with EPBs and may be produced by direct energetic particle precipitation and/or storm-induced large-scale plasma density gradients. They appear to expand toward the equator to ~30°N (dip lat. 36°N) with a structure
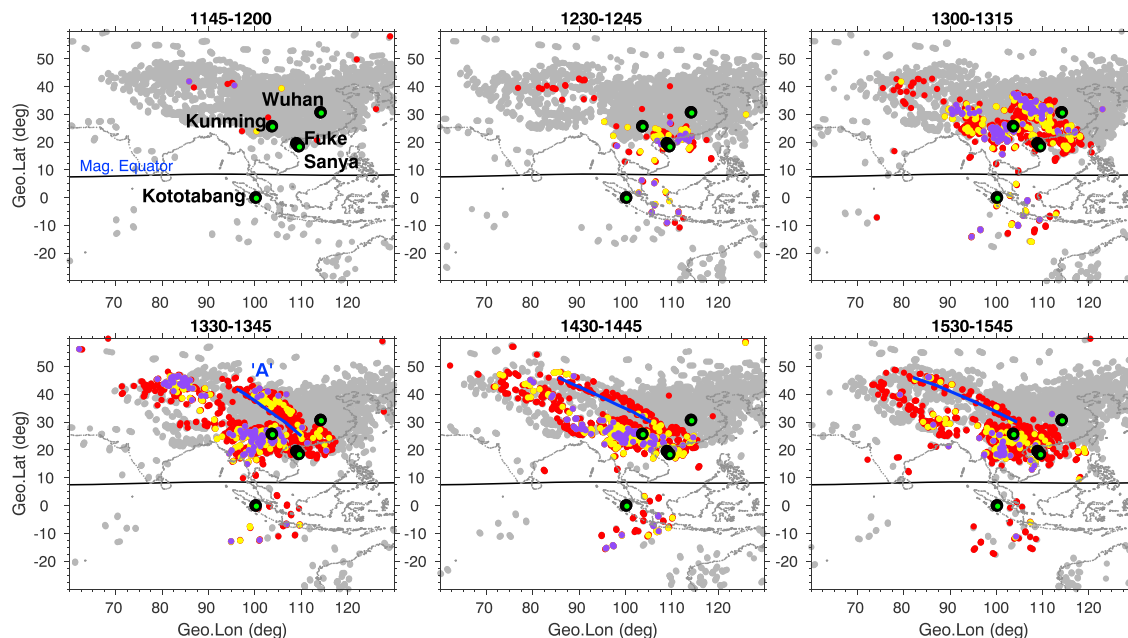
Figure 6. Rate of total electron content change index maps at selected time intervals (on 8 September) in the Asian sector. The black circles with green dots mark the locations of the very high frequency radars. The superimposed blue curve in the bottom panel represents the west wall of the west-tilted structure "A."
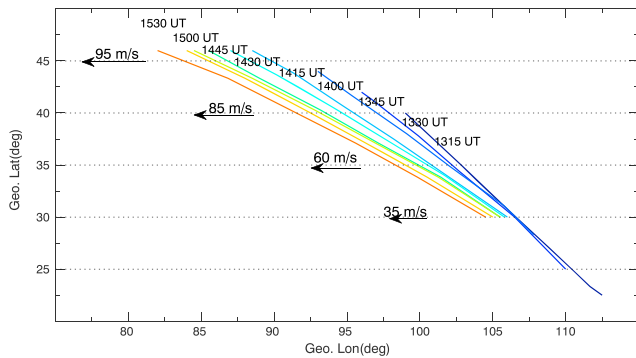
Figure 7. The positions of the west-tilted structure "A" (shown in Figure 6) at different time intervals. The drift velocities at four selected latitudes (30°N, 35°N, 40°N, 45°N) were estimated, about 35, 60, 85, and 95 m/s, respectively.

aligned along the northwest-southeast direction (marked with black slant lines in Figure 5), in a pattern similar to that of the storm-enhanced density (e.g., Foster et al., 2005). The structure disappeared around 0400 UT. The other type of irregularities initially observed over the equatorial station Fortaleza (and Jicamarca) are associated with EPBs which began development following the first southward excursion of IMF Bz and became further intensified following the southward intensification of the Bz (around 2310 UT). It is relevant to mention here that the occurrence of quiet time postsunset EPBs over Fortaleza is low in early September, especially under the low solar flux conditions (e.g., Abdu, Sobral, et al., 1998). The EPBs over the longitudes around Fortaleza and Jicamarca grew vertically and extended along magnetic field lines to low latitudes of ~25°S and 40°S, respectively.

In the Asian sector, two main features of irregularities can be noted from the ROTI maps in Figure 6. One is that the irregularities initially appeared at low latitudes around 1230 UT on 8 September, following the second event of the IMF Bz southward excursion. These low-latitude irregularities are associated with EPBs. An obvious longitudinal gradient in the ROTI intensities was observed in the eastern China (starting at 1300 UT), indicating that the EPB occurrence was confined at longitudes westward of ~120°E. We examined this feature by using the backscatter echo observations from a VHF radar network that consisted of the radars located at Wuhan, Sanya, Fuke, Kunming, and Kototabang. The radar locations are shown as bold (green in black circle) dots in Figure 6. The occurrences of EPBs shown in the ROTI maps are, in general, consistent with that observed by the radar network, in that the EPB backscatter plumes were detected over Sanya, Fuke, Kunming, and Kototabang (Figure 8), but not over Wuhan (figure not shown here).

Another feature seen from Figure 6 is that the EPB irregularities were observed extending from low to middle latitudes, with apparent west-tilted structures. The occurrence of middle latitude plasma bubbles during geomagnetic storms is not a rare phenomenon over China and adjacent longitudes, as reported by Li et al. (2009) and Sahai et al. (2009) where EPBs were detected at dip lat. 45°N. The west-tilted structures shown in Figure 6 were presented in Aa et al. (2018). They, however, did not address how the west-tilted structure was formed. Going back to Figure 5, one may note that the shape of the band-like structure observed in the American sector is similar to that of the west-tilted structure observed in the Asian sector. The two types of structures, however, are related to different processes at high and low latitudes, respectively. The west-tilted structures in the Asian sector, which were seen growing from low to middle latitudes during the period 1300–1345 UT, are associated with EPBs. The blue solid curves shown in the bottom panels of Figure 6 mark the west wall of the west-tilted structure labeled "A." To get the zonal drift velocities, Figure 7 shows the positions (of the west wall) of the west-tilted structure A at different intervals during 1315–1530 UT. Based on the change in positions, we have calculated the mean westward velocities of the structure A at different latitudes, which are about 35, 60, 85, and 95 m/s, at 30°N, 35°N, 40°N, and 45°N, respectively. The results show that there is a latitudinal gradient in the westward drifts.

At lower latitudes less than 30°N, the zonal drifts of EPBs cannot be resolved from the present ROTI maps. In Figure 8, we show the details of backscatter echoes obtained from the Kunming, Fuke, Sanya, and Kototabang VHF radars. The echo intensities obtained from the northward/southward beams of the Kunming, Fuke, Sanya, and Kototabang radars are shown as a function of height and time. The corresponding apex altitudes over the magnetic equator in the longitude where the radar is located are superimposed in the left of each panel. In general, periodic EPB backscatter echoing groups, which occurred around 1330–1830 UT, 1230–1800 UT, 1230–1800 UT, and 1230–2200 UT on 8 September, were detected by these radars, respectively. The periodic EPBs shown in the radar height-time-intensity plots are due to spatially separated EPBs traversing through the radar field of view (FOV; e.g., Li et al., 2013). Notably, the first EPB groups detected by the Sanya, Fuke, and Kototabang radars were freshly generated in the radar FOV near simultaneously, around 1230 UT, and extended up to ~800-km apex altitude. It could be that the same external forcing drove the generation of EPBs simultaneously over the radar longitudes separated by about 1,000 km. For the other groups of EPBs observed by these radars, they appeared first in the eastern beams and drifted westward out of the radar FOV. The descending structures of backscatter echoes after ~1500 UT may be resulting from the westward drift of west-tilted EPBs. Figure 9 shows the echo intensity zonal distribution (positive values
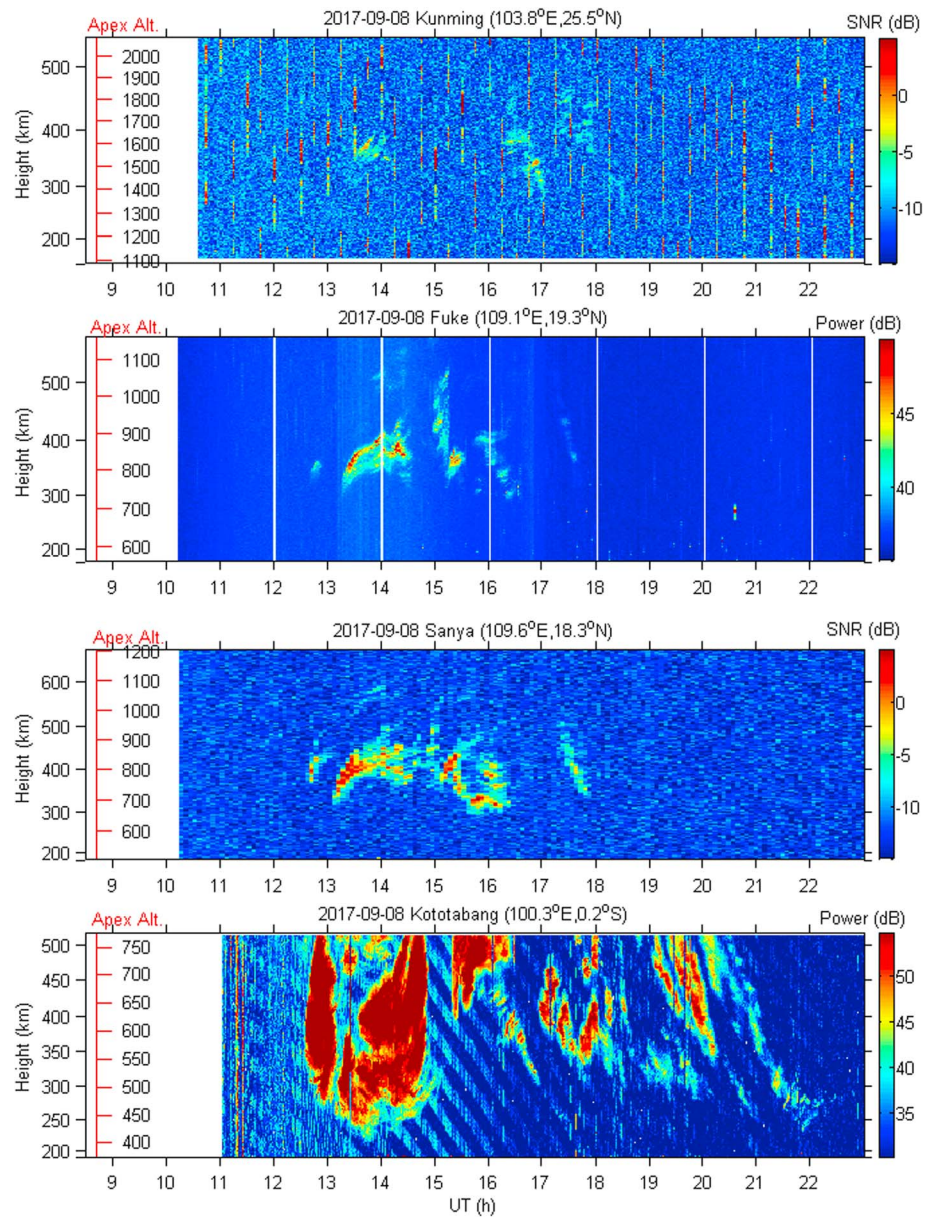
Figure 8. Height-time-intensity maps of backscatter echoes obtained from the Kunming, Fuke, Sanya, and Kototabang very high frequency radars on 8 September 2017. For each radar, the corresponding apex altitude over the magnetic equator (calculated by tracing the magnetic field line to its apex using IGRF-2015) is also shown in the left of each panel.

represent the east) at 380-km altitude as observed by the Kototabang radar 16-beam steering measurements during 1200–2300 UT on 8 September. All echo groups have negative slopes, indicating westward drifts of the EPB groups. From the slopes shown in Figure 9, the drift velocities of different EPB groups were estimated by linear fitting, ranging ~40–70 m/s (westward).

4. Discussion

Equatorial plasma bubbles are widely accepted to be generated at low latitudes around the magnetic equator through the generalized Rayleigh-Taylor (R-T) instability mechanism (Kelley, 2009). The growth rate of R-T instability depends on a few factors, including the external driving forces, for example, the zonal electric field, and the background ionospheric properties (e.g., Abdu, 2001, and references therein). Earlier studies on the
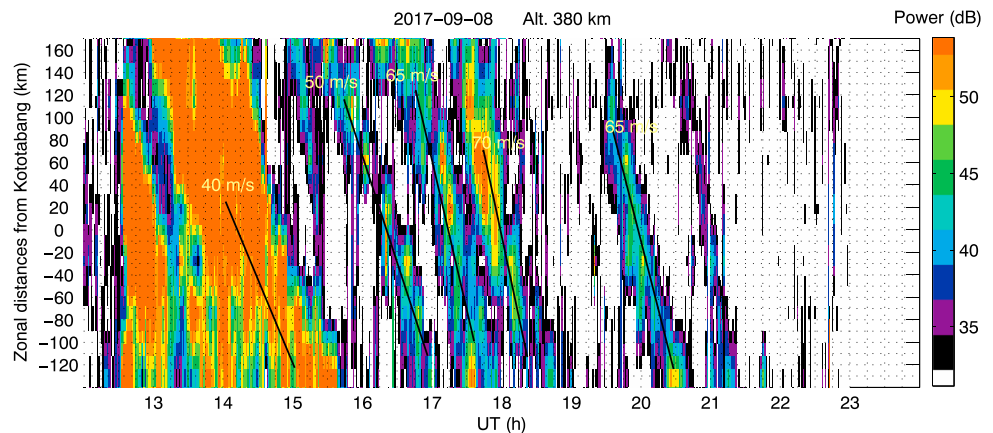
Figure 9. Echo intensity by the Kototabang radar 16-beam steering measurements at 380-km altitude during 1200–2300 UT on 8 September 2017, as a function of zonal distance (positive values represent the east) and time. The superimposed black slant line represents the slope of linear fitting employed for the calculation of zonal drift (from left to right: 40, 50, 65, 70, and 65 m/s westward).

longitudinal/seasonal distributions of EPBs have shown that the prereversal enhancement of eastward electric field (PRE) around sunset plays a dominant role on the generation of postsunset EPBs (e.g., Fejer et al.,1999; Huang, 2018; Li et al., 2007). Under the action of PRE, the ionosphere is rapidly elevated to high altitudes where the ion-neutral collision frequency decreases. The growth rate for the R-T instability therefore enhances with increasing height. On geomagnetic quiet days, the intensity of PRE is usually thought to be controlled by the sunset E region conductivity longitudinal gradient and the thermospheric zonal wind (Kelley, 2009).

During geomagnetic storm periods, and under southward IMF Bz excursions, the magnetospheric/high latitude electric field promptly penetrates to the equatorial ionosphere as under-shielding electric field (PPEF), with its duration varying from tens of minutes to several hours. A few hours from the beginning of the PPEFs, the DDEF may develop. By using the ROCSAT-1 measurements during 1999–2005, Fejer et al. (2008) investigated the local time variations of longitudinally averaged vertical plasma drifts driven by storm time disturbance electric fields. It was found that the PPEF has eastward polarity during daytime extending into postsunset hours, with the maximum amplitude around sunset (1800–1900 LT), in phase with the PRE development. The DDEF, however, has its polarity opposite to that of the PPEF. These storm time electric fields can significantly alter the equatorial ionospheric electric fields. For example, a PPEF (DDEF) occurring at sunset hours may significantly enhance (decrease) the PRE vertical drift, thereby enhancing (suppressing) the generation of postsunset EPBs (Abdu, 2012, and references therein). According to the local time/longitudinal variation pattern of PPEF and DDEF, the development of postsunset EPBs, if enhanced in a longitude sector by the PPEF, will usually be inhibited in its western longitudes by the DDEF that may occur after some time delay. In this regard, it may be recalled that earlier investigations have shown substantial differences in the storm time EPB activities at close-by longitudinal sectors (e.g., Basu et al., 2001).

For the storm event of 7–8 September, the postsunset EPBs were significantly enhanced at two longitude sectors separated by ~180° (Figure 3). In order to understand how the geomagnetic storm affected the EPB development, leading to the generation of postsunset EPBs in the American and Asian sectors, and the absence in the Pacific sector, respectively, the F layer peak heights (hmF2) obtained from the equatorial and low-latitude ionosondes at Fortaleza, Jicamarca, Guam, and Sanya, together with the IMF Bz component, are plotted in Figure 10. For comparison, the hmF2 observations on the geomagnetic quiet day 6 September are shown as gray lines. The superimposed blue axis in the bottom of each panel represents the local time. The shaded regions mark the sunset hours 1800–2000 LT at the different locations.

Figure 10b shows that during the southward excursion of IMF Bz on 7 September, the hmF2 over Fortaleza moved upward slowly (several meters per second) instead of downward (on the quiet day). Over Jicamarca and Guam (Figures 10c and 10d), the hmF2 increased abruptly with a large amplitude. The corresponding vertical drifts of F layer were estimated, on average, to be 43 and 20 m/s, respectively. The drift reversal
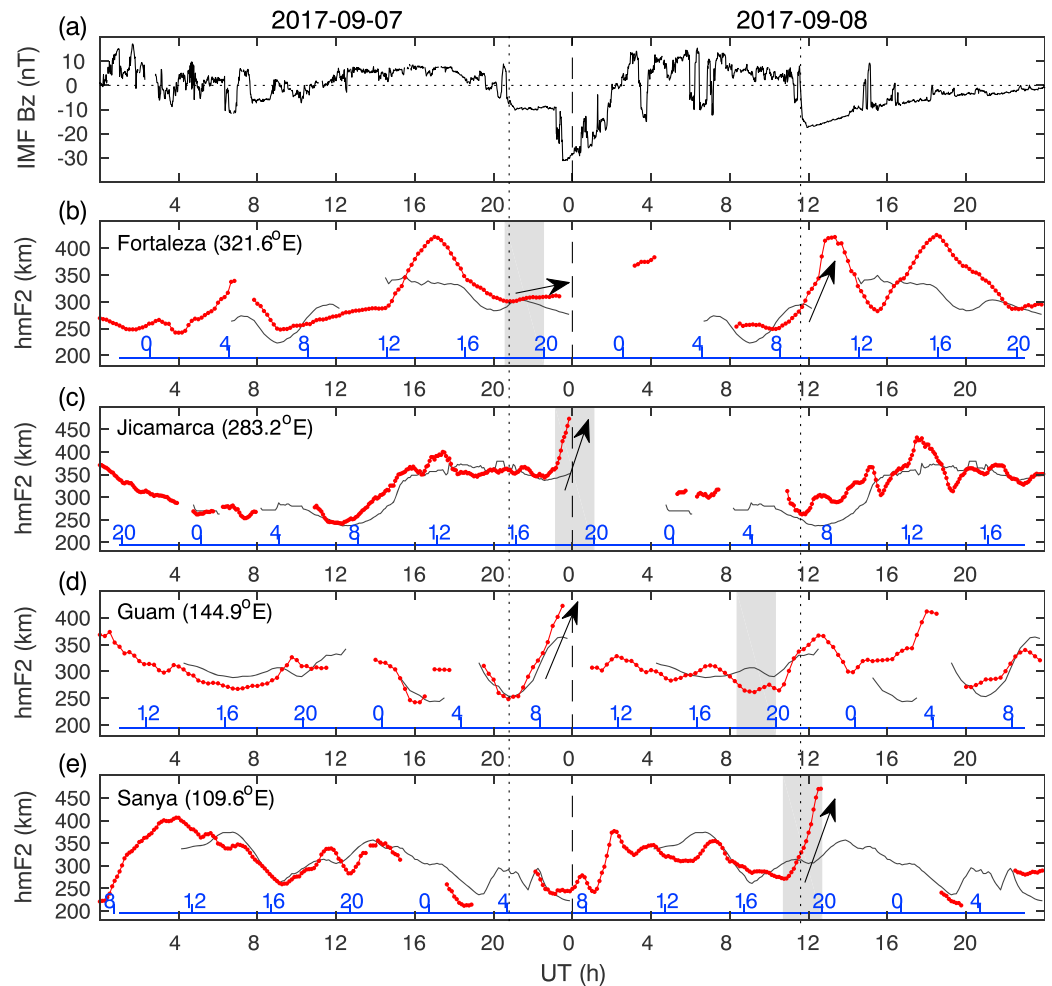
Figure 10. (a–e) The variations of interplanetary magnetic field *Bz* and of ionospheric hmF2 observed at Fortaleza, Jicamarca, Guam, and Sanya on 7–8 September 2017. The gray lines are geomagnetic quiet day (6 September 2017) values. The shaded region marks the sunset hours (1800–2000 LT).

(Fortaleza) and abrupt increase (Jicamarca and Guam), as compared to that on the quiet day, suggest the presence of an enhanced eastward electric field, which resulted from the PPEF due to the southward IMF. The PPEF efficiency (at equatorial latitudes) and therefore its amplitude is local time dependent (e.g., Fejer et al., 2008), having largest amplitude at sunset hours as may be noted in the significantly enhanced PRE vertical drift over Jicamarca (that was caused by the in-phase superposition of the PPEF with the normal PRE vertical drift during sunset hours). The enhanced PRE moved the *F* layer to higher altitudes with a larger upward velocity, where the ion-neutral collision frequency and the flux tube recombination rate are lower that could cause a more rapid growth rate of the R-T instability, leading to intense EPB activities that quickly grew in altitude and extended to higher latitudes in the American sector (Figure 5).

In contrast, in the pacific sector, postsunset EPB/ESF did not develop. Over Guam, the sunset occurred about 10 hr after the PPEF episode, by which time the DDEF driven by disturbance thermospheric winds due to auroral heating could be present with opposite polarity (westward), suppressing or even reversing the normal PRE. From the local time variation pattern of DDEF shown in Figure 2 of Fejer et al. (2008), it is evident that the plasma vertical drift due to DDEF is downward with maximum intensity in the postsunset hours. As shown in Figure 10d, the sunset hmF2 (indicative of the PRE vertical drift) did not present any rise over Guam. In fact, the hmF2 was lower than that on a normal day. Because of larger ion-neutral collision frequency at lower altitudes, the growth rate of the R-T instability becomes smaller there. As a result, the postsunset ESF development was inhibited/not triggered over Guam.

We now consider the storm effects on the EPBs in the Asian sector. The hmF2 observations over Sanya are shown in Figure 10e. It can be noted that on 8 September, an abrupt increase in hmF2 started around sunset, with a mean upward velocity of about 37 m/s over Sanya. Compared to the geomagnetic quiet day, the PRE on 8 September over the Sanya longitude is significantly enhanced, following the second southward turning of the IMF Bz. It is relevant to mention that the southward turning caused a large increase in hmF2 also over Fortaleza in the morning hours. Examination of the radar backscatter observations presented in Figure 8 shows that on 8 September, the postsunset EPBs began almost simultaneously, around 1230 UT over Sanya, Fuke, and Kototabang. Under geomagnetic quiet conditions, the onset of postsunset EPBs driven by normal PRE over Kototabang (located westward of Sanya) is normally delayed by about 30 min with respect to that over Sanya (e.g., Li et al., 2016). The simultaneous onset of postsunset EPBs over the two longitudes (separated by ~1,000 km) indicates that the developments of these EPBs should be driven by the same external forcing, that is, the PPEFs associated with the second (12 UT) southward turning of IMF Bz. Considering that the storm started more than 12 hr earlier, a westward DDEF could continue to exist near sunset in the Asia sector, at the time of the second PPEF episode. This indicates that the impact of the PPEFs was strong enough to overcome that of the possible DDEFs and to cause the large upward drifts around sunset. This large upward drift produced the intense EPB irregularities that expanded significantly to middle latitude (Figure 6).

Another issue is the formation of west-tilted irregularity structure in the Asian sector. During geomagnetic quiet conditions, the normally eastward thermospheric wind at nighttime causes downward electric field that usually predominates in the nighttime ionosphere driving the plasma drift also eastward with nearly similar velocities. The eastward winds (obtained from the HWM model) often decrease with increasing latitude, from more than hundreds (at low latitude) to several tens of meters per second (at middle latitude). Correspondingly, the plasma eastward drift velocity decreases with increasing altitude/latitude. By using all-sky airglow imager observations in Brazil and the HWM-90 model, Pimenta et al. (2003) reported that the latitudinal variation of EPB zonal drifts correspond well with that of the HWM zonal winds. Such altitude/latitude variation of eastward drifts were suggested to be responsible for the west-tilted structure (or backward C-shapes) in eastward drifting EPB images from optical observations (e.g., Kil et al., 2009; Otsuka et al., 2002). However, in the present case the west-tilted structures drifted toward the west, which is in contrast to the eastward drift of quiet time west-tilted EPBs. As shown in Figure 7, the westward drift velocity at middle and low latitudes are about 95 and 35 m/s, respectively, which clearly suggests that west-tilted structures in the present case are not due to the decrease in the plasma drift with latitude/altitude, but rather result from the increased westward drifts with latitude/altitude.

As regarding the mechanisms responsible for the westward drifts of storm time irregularities, there are several possibilities, including the PPEF-induced Hall drifts, and the disturbance westward thermospheric winds, which dominate, respectively, during AE activity under southward IMF Bz conditions, and during the storm recovery phase (e.g., Abdu, 2012; Abdu, Jayahandran, et al., 1998; Emmert et al., 2004; Fejer & Scherliess, 1998). Using ion drift observations from the DE-2 satellite, Fejer and Scherliess (1998) studied the latitudinal and temporal variations of plasma zonal drifts driven by PPEFs at middle and low latitudes. They showed that during the initial time (t_0 + 30 min) of AE intensification (by about 220 nT), the prompt penetration plasma zonal drifts are predominantly westward, with largest amplitude in the dusk sector, the amplitude decreasing toward lower latitudes. A possible contribution to the westward drift from the Hall conduction effect is not explicit in their observation. However, with increasing storm time, the disturbance thermospheric zonal wind driven by enhanced energy deposition into the high-altitude ionosphere can also change the middle- and low-latitude drift patterns. Such modification may result from the fact that the disturbance thermospheric winds, during their equator-ward propagation, acquire westward momentum due to the Coriolis effect dominating at midlatitudes. From analysis of CHAMP data during the geomagnetic storm of 29 October 2003, Sutton et al. (2005) found westward enhancement of thermospheric winds at middle and low latitudes. We further note in this regard that based on the CHAMP zonal wind observations during 2001–2005, Xiong et al. (2015) investigated the local time and latitudinal variations of disturbance thermospheric zonal wind. They found that the disturbance westward wind propagated from high to low latitudes, with peak values of 200, 80, and 50 m/s at subauroral, middle, and equatorial latitudes, respectively. The westward drifts of irregularities increasing from low to middle latitudes, occurring more than 12 hr after the storm onset, as inferred in the Asia sector in the present case, are in very good agreement with the latitude-dependent characteristics

of the disturbance thermospheric wind observed in the CHAMP satellite data. On the other hand, the fact that the second southward excursion of IMF Bz occurred during the same period might imply that a possible source of the westward drifts arising from the PPEFs could also contribute to the observed disturbance westward drift. The separation of the two components of the disturbance westward drift is not attempted here.

5. Conclusions

Based on the data mainly from a series of GNSS TEC receivers, VHF radars, and ionosondes around the approximate meridian 120°E/60°W, the present study of EPBs developments in the Asian, Pacific, and American longitude sectors, during the geomagnetic storm of 7–8 September 2017, leads to the following conclusions.

1. The EPB development, following the sunset terminators, became significantly enhanced in the American and Asian sectors, where the rapid vertical growth of the bubble structures resulted in latitudinal extension of the TEC depletion structures to low and midlatitudes of ~ dip lat. 30°N and 46°N, respectively. In contrast to this the EPB development was inhibited in the Pacific sector.
2. The undershielding PPEFs of eastward polarity associated with the two episodes of rapid southward turnings of IMF, producing two main phase decreases separated between them by ~15 hr in local time, modulated the sunset rise of the F layer (and PRE vertical drift) that led to the enhanced development of EPBs in the American and Asian sectors.
3. The postsunset EPB development in the Pacific sector was suppressed during the recovery phase of the earlier storm (corresponding to the first main phase decrease) due to DDEF that prevailed with westward polarity in the sunset sector over this longitude.
4. Whereas the EPBs in both the American and Asian sectors were generated through the PPEF-predominated R-T instability process, they, however, show different characteristics, with apparent west-tilted structure in the Asian sector but not in the American sector.
5. In the Asian sector, the EPBs were observed to drift westward during postsunset hours. While the thermospheric disturbance westward wind originating from the earlier storm episode may be suggested to drive the storm time westward plasma drift, the role of prompt penetration induced plasma westward drifts, however, cannot be ruled out.
6. The west-tilted structure of irregularities observed in the Asian sector indicated the role of pole-ward increasing westward plasma drifts, instead of pole-ward decreasing plasma drift reported previously (for quiet conditions).

For the present case, the zonal drifts of EPBs in the American sector could not be obtained. It is worth to mention that westward/decreased eastward EPB drifts driven by PPEFs have been frequently observed over American sector, in contrast to their rare occurrence in East Asia. Whereas this study brings out some important aspects of the significantly enhanced postsunset EPB development along the ~120°E/60°W meridian, and the increased westward drifts of the EPBs with latitude around 120°E in response to geomagnetic storms, many details are still not clear, as to how the different the storm time EPBs evolve in the two longitude sectors. More detailed investigation could be achieved in future by using additional instruments being developed, for example, the Ionospheric Observation Network for Irregularity and Scintillation in East/Southeast Asia, which consists of two chains along the 110°E and 23°N, and the Low-latitude Ionospheric Sensor Network in South America, to resolve the fine structure of EPBs.

References

Aa, E., Huang, W., Liu, S., Ridley, A., Zou, S., Shi, L., et al. (2018). Midlatitude plasma bubbles over China and adjacent areas during a magnetic storm on 8 September 2017. *Space Weather*, *16*, 321–331. https://doi.org/10.1002/2017SW001776

Abdu, M. A. (2001). Outstanding problems in the equatorial ionosphere thermosphere electrodynamics relevant to spread F. *Journal of Atmospheric and Solar - Terrestrial Physics*, *63*(9), 869–884. https://doi.org/10.1016/S1364-6826(00)00201-7

Abdu, M. A. (2012). Equatorial spread F/plasma bubble irregularities under storm time disturbance electric fields. *Journal of Atmospheric and Solar - Terrestrial Physics*, *75-76*, 44–56. https://doi.org/10.1016/j.jastp.2011.04.024

Abdu, M. A., Batista, I. S., Takahashi, H., MacDougall, J., Sobral, J. H., Medeiros, A. F., & Trivedi, N. B. (2003). Magnetospheric disturbance induced equatorial plasma bubble development and dynamics: A case study in Brazilian sector. *Journal of Geophysical Research*, *108*(A12), 1449. https://doi.org/10.1029/2002JA009721

Abdu, M. A., Jayahandran, P. T., MacDougall, J., Cecile, J. F., & Sobral, J. H. A. (1998). Equatorial F region zonal plasma irregularity drifts under magnetospheric disturbances. *Geophysical Research Letters*, *25*(22), 4137–4140. https://doi.org/10.1029/1998GL900117

Abdu, M. A., Sobral, J. H. A., Batista, I. S., Rios, V. H., & Medina, C. (1998). Equatorial spread-F occurrence statistics in the American longitudes: Diurnal, seasonal and solar cycle variations. *Advances in Space Research*, *22*(6), 851–854. https://doi.org/10.1016/S0273-1177(98)00111-2

Basu, S., Basu, S., Valladares, C. E., Yeh, H. C., Su, S. Y., MacKenzie, E., et al. (2001). Ionospheric effects of major magnetic storms during the International Space Weather Period of September and October 1999: GPS observations, VHF/UHF scintillations, and in situ density structures at middle and equatorial latitudes. *Journal of Geophysical Research*, *106*(A12), 30,389–30,413. https://doi.org/10.1029/2001JA001116

Basu, S., Basu, S., MacKenzie, E., Bridgwood, C., Valladares, C. E., Groves, K. M., & Carrano, C. (2010). Specification of the occurrence of equatorial ionospheric scintillations during the main phase of large magnetic storms within solar cycle. *Radio Science*, *45*, RS5009. https://doi.org/10.1029/2009RS004343

Carter, B. A., Yizengaw, E., Pradipta, R., Retterer, J. M., Groves, K., Valladares, C., et al. (2016). Global equatorial plasma bubble occurrence during the 2015 St. Patrick's Day storm. *Journal of Geophysical Research: Space Physics*, *121*, 894–905. https://doi.org/10.1002/2015JA022194

Cherniak, I., & Zakharenkova, I. (2016). First observations of super plasma bubbles in Europe. *Geophysical Research Letters*, *43*, 11,137–11,145. https://doi.org/10.1002/2016GL071421

Emmert, J. T., Fejer, B. G., Shepherd, G. G., & Solheim, B. H. (2004). Average nighttime F region disturbance neutral winds measured by UARS WINDII: Initial results. *Geophysical Research Letters*, *31*, L22807. https://doi.org/10.1029/2004GL021611

Fejer, B. G., Jensen, J. W., & Su, S.-Y. (2008). Quiet time equatorial F region vertical plasma drift model derived from ROCSAT-1 observations. *Journal of Geophysical Research*, *113*, A05304. https://doi.org/10.1029/2007JA012801

Fejer, B. G., & Scherliess, L. (1998). Mid- and low-latitude prompt-penetration ionospheric zonal plasma drifts. *Geophysical Research Letters*, *25*(16), 3071–3074. https://doi.org/10.1029/98GL02325

Fejer, B. G., Scherliess, L., & de Paula, E. R. (1999). Effects of the vertical plasma drift velocity on the generation and evolution of equatorial spread F. *Journal of Geophysical Research*, *104*, 19,859–19,869.

Foster, J. C., Coster, A. J., Erickson, P. J., Holt, J. M., Lind, F. D., Rideout, W., et al. (2005). Multiradar observations of the polar tongue of ionization. *Journal of Geophysical Research*, *110*, A09S31. https://doi.org/10.1029/2004JA010928

Fukao, S., Ozawa, Y., Yamamoto, M., & Tsunoda, R. T. (2003). Altitude extended equatorial spread F observed near sunrise terminator over Indonesia. *Geophysical Research Letters*, *30*(22), 2137. https://doi.org/10.1029/2003GL018383

Ghodpage, R. N., Patil, P. T., Gurav, O. B., Gurubaran, S., & Sharma, A. K. (2018). Ionospheric response to major storm of 17th March 2015 using multi-instrument data over low latitude station Kolhapur (16.8°N, 74.2°E, 10.6°dip. Lat.). *Advances in Space Research*, *62*(3), 624–637. https://doi.org/10.1016/j.asr.2018.05.003

Huang, C.-S. (2018). Effects of the postsunset vertical plasma drift on the generation of equatorial spread F. *Progress in Earth and Planetary Science*, *5*(1), 3. https://doi.org/10.1186/s40645-017-0155-4

Jin, H., Zou, S., Chen, G., Yan, C., Zhang, S., & Yang, a. G. (2018). Formation and evolution of low-latitude F region field-aligned irregularities during the 7–8 September 2017 storm: Hainan coherent scatter phased array radar (HCOPAR) and Hainan digisonde observations. *Space Weather*, *16*, 648–659. https://doi.org/10.1029/2018SW001865

Katamzi-Joseph, Z. T., Habarulema, J. B., & Hernández-Pajares, M. (2017). Midlatitude postsunset plasma bubbles observed over Europe during intense storms in April 2000 and 2001. *Space Weather*, *15*, 1177–1190. https://doi.org/10.1002/2017SW001674

Kelley, M. C. (2009). *The Earth's ionosphere: Plasma physics and electrodynamics, Int. Geophys. Ser.* (Vol. 43). San Diego, CA: Academic Press.

Kil, H., Heelis, R. A., Paxton, L. J., & Oh, S.-J. (2009). Formation of a plasma depletion shell in the equatorial ionosphere. *Journal of Geophysical Research*, *114*, A11302. https://doi.org/10.1029/2009JA014369

Lei, J., Huang, F., Chen, X., Zhong, J., Ren, D., Wang, W., et al. (2018). Was magnetic storm the only driver of the long-duration enhancements of daytime total electron content in the Asian-Australian sector between 7 and 12 September 2017? *Journal of Geophysical Research: Space Physics*, *123*, 3217–3232. https://doi.org/10.1029/2017JA025166

Li, G., Ning, B., Abdu, M. A., Otsuka, Y., Yokoyama, T., Yamamoto, M., & Liu, L. (2013). Longitudinal characteristics of spread F backscatter plumes observed with the EAR and Sanya VHF radar in Southeast Asia. *Journal of Geophysical Research: Space Physics*, *118*, 6544–6557. https://doi.org/10.1002/jgra.50581

Li, G., Ning, B., Abdu, M. A., Wan, W., Wang, C., Yang, G., et al. (2017). First observation of presunset ionospheric F region bottom type scattering layer. *Journal of Geophysical Research: Space Physics*, *122*, 3788–3797. https://doi.org/10.1002/2016JA023647

Li, G., Ning, B., Hu, L., Liu, L., Yue, X., Wan, W., et al. (2010). Longitudinal development of low-latitude ionospheric irregularities during the geomagnetic storms of July 2004. *Journal of Geophysical Research*, *115*, A04304. https://doi.org/10.1029/2009JA014830

Li, G., Ning, B., Liu, L., Ren, Z., Lei, J., & Su, S.-Y. (2007). The correlation of longitudinal/seasonal variations of evening equatorial pre-reversal drift and of plasma bubbles. *Annales de Geophysique*, *25*(12), 2571–2578. https://doi.org/10.5194/angeo-25-2571-2007

Li, G., Ning, B., Zhao, B., Liu, L., Wan, W., Ding, F., et al. (2009). Characterizing the 10 November 2004 storm-time middle-latitude plasma bubble event in Southeast Asia using multi-instrument observations. *Journal of Geophysical Research*, *114*, A07304. https://doi.org/10.1029/2009JA014057

Li, G., Otsuka, Y., Ning, B., Abdu, M. A., Yamamoto, M., Wan, W., et al. (2016). Enhanced ionospheric plasma bubble generation in more active ITCZ. *Geophysical Research Letters*, *43*, 2389–2395. https://doi.org/10.1002/2016GL068145

Ma, G., & Maruyama, T. (2006). A super bubble detected by dense GPS network at east Asian longitudes. *Geophysical Research Letters*, *33*, L21103. https://doi.org/10.1029/2006GL027512

Nishioka, M., Saito, A., & Tsugawa, T. (2008). Occurrence characteristics of plasma bubble derived from global ground-based GPS receiver networks. *Journal of Geophysical Research*, *113*, A05301. https://doi.org/10.1029/2007JA012605

Otsuka, Y., Shiokawa, K., Ogawa, T., & Wilkinson, P. (2002). Geomagnetic conjugate observations of equatorial airglow depletions. *Geophysical Research Letters*, *29*(15), 1753. https://doi.org/10.1029/2002GL015347

Patra, A. K., Chaitanya, P. P., Dashora, N., Sivakandan, M., & Taori, A. (2016). Highly localized unique electrodynamics and plasma irregularities linked with the 17 March 2015 severe magnetic storm observed using multitechnique common-volume observations from Gadanki, India. *Journal of Geophysical Research: Space Physics*, *121*, 11,518–11,527. https://doi.org/10.1002/2016JA023384

Pi, X., Mannucci, A. J., Lindqwister, U. J., & Ho, C. M. (1997). Monitoring of global ionospheric irregularities using the worldwide GPS network. *Geophysical Research Letters*, *24*(18), 2283–2286. https://doi.org/10.1029/97GL02273

Pimenta, A. A., Fagundes, P. R., Sahai, Y., Bittencourt, J. A., & Abalde, J. R. (2003). Equatorial F-region plasma depletion drifts: Latitudinal and seasonal variations. *Annales de Geophysique*, *21*(12), 2315–2322. https://doi.org/10.5194/angeo-21-2315-2003

Sahai, Y., Becker-Guedes, F., Fagundes, P. R., de Jesus, R., de Abreu, A. J., Otsuka, Y., et al. (2009). Effects observed in the ionospheric F region in the east Asian sector during the intense geomagnetic disturbances in the early part of November 2004. *Journal of Geophysical Research*, *114*, A00A18. https://doi.org/10.1029/2008JA013053

Santos, A. M., Abdu, M. A., Souza, J. R., Sobral, J. H. A., Batista, I. S., & Denardini, C. M. (2016). Storm time equatorial plasma bubble zonal drift reversal due to disturbance Hall electric field over the Brazilian region. *Journal of Geophysical Research: Space Physics*, *121*, 5594–5612. https://doi.org/10.1002/2015JA022179

Sutton, E. K., Forbes, J. M., & Nerem, R. S. (2005). Global thermospheric neutral density and wind response to the severe 2003 geomagnetic storms from CHAMP accelerometer data. *Journal of Geophysical Research*, *110*, A09S40. https://doi.org/10.1029/2004JA010985

Tulasi Ram, S., Rama Rao, P. V. S., Prasad, D. S. V. V. D., Niranjan, K., Gopi Krishna, S., Sridharan, R., & Ravindran, S. (2008). Local time dependent response of postsunset ESF during geomagnetic storms. *Journal of Geophysical Research*, *113*, A07310. https://doi.org/10.1029/2007JA012922

Wang, C. (2010). New chains of space weather monitoring stations in China. *Space Weather*, *8*, S08001. https://doi.org/10.1029/2010SW000603

Xiong, C., Lühr, H., & Fejer, B. G. (2015). Global features of the disturbance winds during storm time deduced from CHAMP observations. *Journal of Geophysical Research: Space Physics*, *120*, 5137–5150. https://doi.org/10.1002/2015JA021302

Zhou, C., Tang, Q., Huang, F., Liu, Y., Gu, X., Lei, J., et al. (2018). The simultaneous observations of nighttime ionospheric E region irregularities and F region mediumscale traveling ionospheric disturbances in midlatitude China. *Journal of Geophysical Research: Space Physics*, *123*, 5195–5209. https://doi.org/10.1029/2018JA025352